Materials Research. 2019; 22(Suppl1): e20180818
DOI: http://dx.doi.org/10.1590/1980-5373-MR-2018-0818

Application of SnO_2 Nanoparticles and Zeolites in Coal Mine Methane Sensors

***Rafael Colombo Abruzzi*[a]*, *Marçal José Rodrigues Pires*[a], *Berenice Anina Dedavid*[a,b], *Camila Fensterseifer Galli*[b]**

[a]*Programa de Pós-Graduação em Engenharia e Tecnologia de Materiais, Pontifícia Universidade Católica do Rio Grande do Sul - PUCRS, Avenida Ipiranga 6681, 90619-900, Porto Alegre, RS, Brasil*
[b]*Escola Politécnica, Pontifícia Universidade Católica do Rio Grande do Sul - PUCRS, Avenida Ipiranga 6681, 90619-900, Porto Alegre, RS, Brasil*

Received: December 07, 2018; Accepted: April 16, 2019

We evaluated solid-state sensors (MOS) manufactured using nanostructured tin oxide (SnO_2) obtained by different synthesis methods for selectivity, response and repeatability at different operating temperatures and methane concentrations. In addition, Zeolite 13X pellets were placed in front of the sensors to improve CH_4 selectivity in the presence of CO_2. The palladium doped sensor (1.4% w/w) showed the highest sensitivity at 80 ºC (83%) and shorter response times (16 s), whereas non-doped sensors exhibited the best sensitivity (78%) and response times (14 s) for those with smaller particle size (8 nm). Zeolite 13X pellets proved to be efficient at making the sensor more selective for CH_4 in the presence of CO_2.

Keywords: *Solid-state sensor, metal-oxide, coal mine atmospheres, CO_2 filter, zeolites.*

1. Introduction

Metal oxides have exceptional potential as basic materials in emerging technologies. Tin oxide (SnO_2), a metallic oxide n-type semiconductor, is one such material that, in presence of intrinsic defects (mainly oxygen vacancies and interstitial Sn atoms) which act with donors (n-type charge carriers), increasing the number of free electrons in the conduction band and consequently the conductivity of the material. The band gap of the intrinsic tin oxide (SnO_2) is of approximately 3.6 eV to 300 K. Its good electrical and electrochemical properties are exploited as catalytic support materials and solid-state chemical sensors[1].

Tin oxide gas sensors (SnO_2) can detect toxic, flammable and explosive gases[2]. In such applications, the response and performance of these devices depends heavily on the size, shape and surface of the active oxide materials, among other factors[1].

Taguchi produced the first generation of commercial gas sensors in Japan in 1960. The low cost of tin oxide makes it highly attractive for gas sensors, but its low sensitivity when it acts at temperatures close to and under the environment makes it difficult to use as a measuring device[2]. Certain factors improve the performance of sensors, including doping with precious metals such as palladium (Pd), which increases the donor population in the conduction band. These metals are excellent efficient oxidation catalysts in addition to improving the surface reactions of sensors, since Pd actively catalyzes molecular oxygen dissociation[3].

Another important factor is the sensor operating temperature, with high temperatures amplifying the kinetics of oxide surface reactions, improving sensor response. However, high temperatures are a complicating factor when these sensors are used to monitor the gas composition in environments containing explosive species because they can trigger an explosion[3,4].

Nanometric oxide particles generate a larger surface, increasing the contact area between the sensor and the target gas, thereby improving the sensitivity of the device[3,5]. In order to enhance sensor selectivity, different alternatives have been studied to eliminate possible atmospheric and humidity-related interferences, including the use of polymer membranes (polyethylene and polypropylene) as a function of differences in analyte permeability[6]. Zeolite films (framework types FAU and MFI) deposited on metal oxides are also under investigation due to the molecular pore size and channel structure of zeolites, which can also adsorb moisture at application sites, such as ambient air in coal mines[7]. For instance, zeolite 13X (FAU type) exhibits a high moisture adsorption capacity, preventing the formation of water vapor water on the surface of the oxide, which affects sensor response properties. The reaction between surface oxygen and water molecules reduces sensor resistance, leading to less adsorption of reactive oxygen species and decreasing the sensitivity of the device[3]. Hugon et al.[8] used zeolite filters on gas sensors to selectively detect methane and n-hexane in the presence of ethanol. These filters could contribute to physically separating the interfering molecules from those of interest, since the sensors react similarly to several substances, which can lead to false alerts.

*e-mail: rafael.abruzzi@acad.pucrs.br

Gases can be hazardous in work environments; for example, methane (CH_4) is one of the most dangerous gases in coal mines due to its explosive potential when mixed with air[9]. The geological processes involved in coal formation produce methane (CH_4) and carbon dioxide (CO_2), which remain trapped in the coal layers until they are exposed and broken up during mining operations[10]. Methane is a combustible gas that emerges from coal seams and is progressively diluted in ventilation air. This dilution reduces its concentration to within the explosive range of 5 to 15%, when it can combust[9]. Thus, there is an urgent need for the development of methane gas sensors with a short response time, good sensitivity and reproducibility close to room temperature[4].

Thus, the present study aims to discuss several methods indicated in the literature for obtaining and synthesizing SnO_2 nanoparticles used to manufacture gas sensors. It describes the step-by-step construction of the sensors and the system used to test them, including GC analysis of the gas in all the tests. Additionally, we analyze the performance of a zeolite 13X filter, placed in front of the sensor, in terms of CH_4 selectivity in a simulated coal mine atmosphere.

2. Material and Methods

2.1. Synthesis and characterization of SnO_2 and zeolite 13X pellets

Table 1 shows the synthesis methods reported in the literature and applied here to produce SnO_2 nanoparticles and construct the gas sensors. SnO_2 was synthesized by $Sn_{(s)}$ oxidation (O1) with HNO_3, as reported by Sergent et al.[11]. The precipitate formed was separated by centrifugation, washed with deionized water and dried at 80 ºC for 24 h and 120 ºC for 15 h. We used two different calcination temperatures, namely 400 ºC (O1A) and 600 ºC (O1B) (10 ºC min^{-1}, 10 h). The SnO_2 nanoparticulate was also synthesized by sol-gel synthesis (O2A), as reported by Senthilkumar et al.[12]. This method involves separating the gel by centrifugation, rinsing with cold deionized water to remove Cl^- ions and drying at 100 ºC. The solids were calcined at 600 ºC (15 ºC min^{-1}, 2 h) for both synthesis methods.

We also performed chemical precipitation (O3) of Pd-doped (O3B) and non-doped (O3A) SnO_2, as proposed by Nandan et al.[13]. Accordingly, we separated the precipitate by filtration, followed by centrifugation, and dried and calcined the product at 80 ºC and 400 ºC (10 ºC min^{-1}, 1 h), respectively. The Pd-doped SnO_2 (O3B) was obtained by adding $PdCl_2$ (1% w/w, Pd) during synthesis.

Commercial SnO_2 nanoparticles (SkySpring Nanomaterials Inc., 50-70 nm) were characterized together, using the same techniques and conditions, in order to comparing them with the samples synthesized in this study.

We used the results of previous tests with different types of zeolites[14] to prepare pellets from commercial zeolite 13X (IQE, Spain). Pelletization was performed to make zeolite easier to handle in determining its efficiency as a possible CO_2 filter on CH_4 sensors to absorb carbon dioxide and water, which interfere in the signal of the device[15]. The pellets were prepared according to the procedure described by Rongsayamanont and Sopajaree[16], by mixing zeolite 13X (Si/Al 1.25) with polyvinyl alcohol (PVA) (15% w/w) and bentonite (9% w/w) in triplicate. The reagents were mixed in a mechanical stirrer (Fisatom Brasil 713D, 4000 rpm), adding deionized water (17.5 mL). The pellets were dried in an oven (60 ºC, 3 h) and activated in a muffle furnace to remove PVA (600 ˚C, 5 ˚C min^{-1}, 3 h). The material was separated based on particle size by sieving, and the fraction between 0.5 and 1.0 mm was used in tests due to its structure.

Sieved SnO_2 powder was analyzed in an XRD-6100 (Shimadzu) diffractometer equipped with a copper tube, to obtain XRD diffractograms. X-ray fluorescence (XRF) analyses were performed in an EDX-7000 diffractometer (Shimadzu) to quantify Pd in the doped SnO_2 (O3B) powder sample. We obtained nitrogen adsorption and desorption isotherms using a Tristar Kr 3020 surface area analyzer (Micromeritics), by previously heating samples (powder) at 120 ºC under vacuum, for 12 h. The specific surface area was determined by the Brunauer, Emmett and Teller (BET) method and pore size distribution using the Barrett, Joyner and Halenda (BJH) method. Semiquantitative SnO_2 analysis was carried out in an Inspect 50 (FEI) scanning electron microscope (FESEM) coupled with energy dispersive X-ray spectroscopy (EDX).

Table 1. Symbology and synthesis conditions for tin oxide and the solid-state sensors produced.

SnO_2 Sample	Method	Calcination Temperature	Sensor	Test Temperature	SnO_2 Thickness
		(ºC)		(ºC)	µm
O1A	Oxidation of $Sn_{(s)}$	400	S1A	80	73
O1B		600	S1B	65	145
O2A	Sol-gel	600	S2A	80	142
O3A	Chemical Precipitation	400	S3A	65	79
*** O3B**		400	S3B[1]	80	44
		400	S3B[2]	50 to 90	75

*Palladium concentration 1 wt%

Particle sizes were calculated using Image J® software and transmission electron microscopy (TEM) images, obtained in a Tecnai G2T20 microscope (FEI) 200 kV.

UV-Vis analyses were carried out to determine the band gap of SnO_2 powder samples, using a UV-2450 spectrophotometer (Shimadzu) in diffuse reflectance mode (DRS). The band gap value was measured by a Tauc plot and the Kubelka-Munk model, considering direct electronic transition between SnO_2 energy bands (n=1/2)[13].

We performed water uptake testing on previously activated (90 min, 400 ºC, 10 ºC min^{-1}) zeolite 13X powder and pellets (~2.0 g) in a closed system to determine moisture adsorption capacity, under controlled atmosphere (20±2 ˚C, relative humidity 85±3%) with NaCl solution (50% w/v). Weight was measured at increasing time intervals (2 min to 48 h) to verify the moisture adsorbed by the zeolite.

2.2. Manufacture of the gas sensors

The SnO_2 nanoparticles were deposited onto platinum electrodes by sputtering (SCD 005 sputter coater, Baltec) on alumina substrates (Al_2O_3) (50 x 10 x 0.58 mm). Similarly, a resistance (150 nm thick) was deposited on the reverse side of the substrate using the heating function of the oxide, as shown in Figure 1. In both cases, we used scanning electron microscopy to assess the deposition quality of trails. AISI 304 stainless steel masks (stencil) were used to obtain the desired geometry for the electrodes and heaters (Supplementary Figure S1), in accordance with Das and Jayaraman[1]. After removing the masks, the assembly was submitted to annealing at 400 ºC to eradicate internal stresses and improve film adherence to the substrate.

The SnO_2 film was deposited on the platinum electrodes by drop coating[17]. To that end, we dispersed SnO_2 powder (1.85% w/w) in an aqueous ethanol solution (15% v/v), which was maintained in an ultrasonic bath for 30 min and then pipetted onto the electrode 5 times.

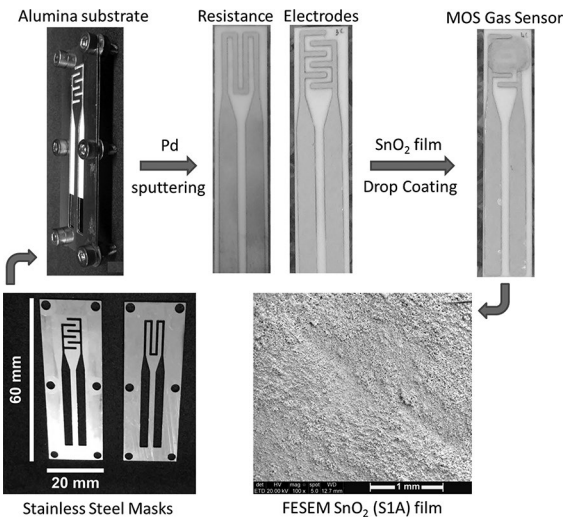

Figure 1. Production system for the sensor with stainless steel masks for sputter deposition of the heaters and platinum electrodes onto the alumina substrate and deposition of the SnO_2 films analyzed by FESEM.

In the case of sensor S3B[1], following resistance tests, three additional drops (30 µL) were deposited (S3B[2]) to increase film thickness. Each drop was evaporated by heating (80 ºC for 30 min). Heat treatment was required after the sequence of depositions (400 ºC, 60 min)[17]. The thickness of the SnO_2 films was measured with a digital specimeter (Ultra Germany).

2.3. Sensor performance tests

Sensor performance tests were carried out in a continuous gas flow system with three gas lines for the three mixtures used: (A) synthetic air (Air Products), (B) 10% CH_4 (Air Products, balanced in N_2) and (C) 15% CO_2 (Air Liquide, balanced in N_2). The system has two gas collection points for sampling aliquots, which were analyzed by gas chromatography (GC-FID) to confirm the actual CH_4 and CO_2 concentrations in the system.

Electrical resistance was measured using a Keithley Source Meter (2400) and data were recorded with Kickstart software. A Teflon device with an O-ring seal (Viton®) was made for heating purposes, with the aid of a DC power supply, and for electrical measurements from the sensor (Figure 2). The heating device was adapted to accommodate a glass tube with gas inlet and outlet connections.

The sensors were tested at different temperatures (20, 50, 65, 80 and 90 ºC), applying a voltage of 10 V[18] using an HK-3003D DC power supply (Hikari). Given the risk of explosion in coal mines, the temperatures used in testing were lower than those reported in the literature for this type of sensor.

In light of the recommended location for sensor use (underground coal mines), we conducted most of the sensor tests within a high concentration range in order to monitor methane at levels close to its explosive range (5 to 15%). In this range, the methane-air mixture can easily ignite when an ignition source is present, causing a violent explosion that can propagate in the presence of combustible coal dust[19]. The tests were performed by varying the methane concentration from 4,000 to 35,000 ppm. Some tests were performed at lower methane concentrations (180 to 3,000 ppm) in order to evaluate sensor sensitivity.

The sensor was also placed in contact with 2,050 ppm of CO_2, followed by 20,109 ppm of CH_4. After these initial tests, the sensor was retested with CO_2 (2,551 ppm) using a previously activated (450 ºC, 10 ºC min^{-1}, 2 h) zeolite 13X pellet filter, subsequently activated *in situ* (100 ºC, 10 ºC min^{-1}, 30 min). Additional testing was then carried out with a mixture of CO_2 (1,699 ppm) and CH_4 (17,197 ppm), applying the zeolite 13X filter and the same activation procedure. The simulate coal mine gases concentration was monitored by gas chromatography (GC) before and after contact with the adsorbent.

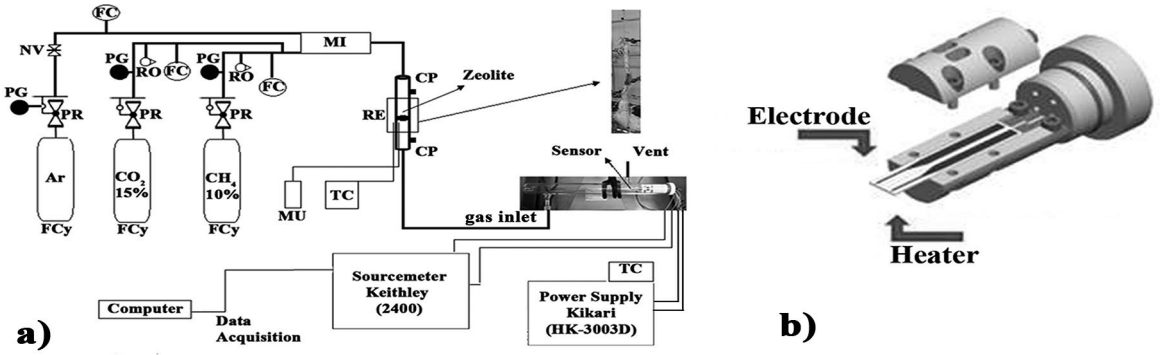

Figure 2. a) Experimental setup to measure sensor response and b) Drawing of the device for measuring the electrical resistance and heating of a solid-state sensor.

The authors[20] conducted prior research to assess different sampling containers and optimize gas chromatography methods, in order to ensure the integrity of gas samples collected and the analytical quality of the results, and lower the costs involved in the process. They suggested a reusable borosilicate glass flask (12 mL), denominated AF-BR, with two septa (PTFE/Silicone + Butyl rubber/PTFE from Supelco) as the best container for sampling GHGs from the ambient air in coal mines. This flask ensured the stability (recovery >95%) of the gases of interest for up to 96 h and showed good reusability (up to 5 evacuation/sampling/analysis cycles without changing septa). Moreover, it performed similarly to the commercial flask, which is 25% more expensive and less readily available.

All the containers studied by[20] were used in previous studies to collect and store gas samples at collection points in coal mines[21]. The gas collection points were chosen in association with ventilation airways. Sampling was carried out at the main entry and return points of the mines, in the ventilation intake and return airways, exhaust, and gas emanation areas. Bonetti et al. (2016) studied the atmospheric CO_2 concentration in coal mines (1,200 ppm on average), which could interfere with CH_4 sensor. As such, tests were performed to assess CO_2 interference and its possible elimination using zeolite 13X pellets. Based on the results obtained in previous tests, the S1A sensor, heated to 80 ºC (10 V), was used for these tests.

The tests lasted 30 min and consisted of three steps: 10 min of synthetic air flow (0.2 to 2 L min^{-1}), 10 min for the analyte of interest (4 to 800 mL $min^{(-1)}$) diluted in synthetic air, and another 10 min of synthetic air. The signal was defined as the change in electrical resistance from an air level (R_a) to a constant level (R_g) when exposed to the target gas, where the response is defined as R_a/R_g[22]. Sensitivity (S%), defined as the variation in electrical resistance before and after contact with the target gas, was calculated by Equation (1)[1].

$$S(\%) = \frac{\Delta R}{R_a} \times 100 = \frac{R_a - R_g}{R_a} \times 100 \qquad (1)$$

Response and recovery times for the gas sensor were defined as the time taken for electrical resistance to reach 90% of its steady state signal after introduction or removal of the analyte.

In all the tests, gas aliquots (15 mL) were collected in triplicate, using a gas tight syringe whenever the gas flow was changed.

The samples were stored in glass flasks for quantification by gas chromatography (GC) of the real gas concentrations the sensor was exposed to. Most studies in the literature do not monitor the actual concentration profile before and after contact with the sensor.

The sampling, storage and analysis of the CO_2 and CH_4, were previously validated[20].

3. Results and Discussion

3.1 Materials characterization

When compared with the commercial oxide (Figure 3 a), XRD characterization of SnO_2 samples synthesized using different processes and calcination temperatures showed diffraction peaks consistent with pure SnO_2 phases (cassiterite crystal structure, tetragonal rutile type) (JCPDS #41-1445), for all the samples analyzed[23]. This finding confirms the results of FTIR analysis, with the presence of bands characteristic of the synthesized material (Supplementary Figure S2). The peaks in Figure 3 (a) show no other impurity-related phases in any of the samples.

We calculated crystallite size using the Scherrer equation; sample O1A exhibited larger crystallites when compared to samples O3A and O3B, synthesized at the same calcination temperature, and sample O1B contained smaller crystallites than O2A. Son and Lee[24] also observed larger crystallites in the oxides calcined at high temperatures (Table 2).

Aziz et al.[25] also reported a rise in SnO_2 calcination temperature, which led to longer and narrower diffraction peaks, related to increased crystallite size and a higher degree of crystallinity. On the other hand, O3B crystallites (doped) were the same size as those in sample O3A (non-doped).

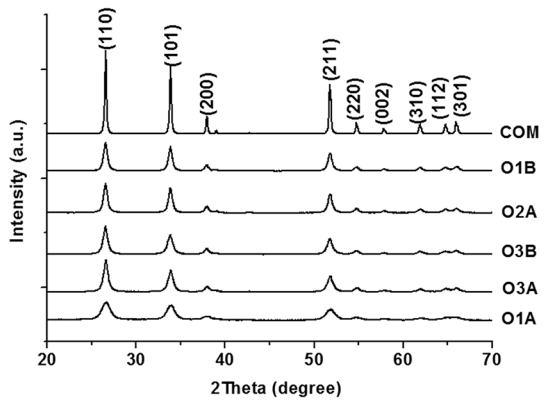

(a)

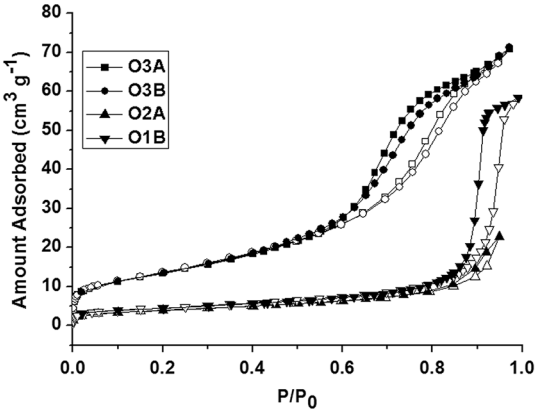

(b)

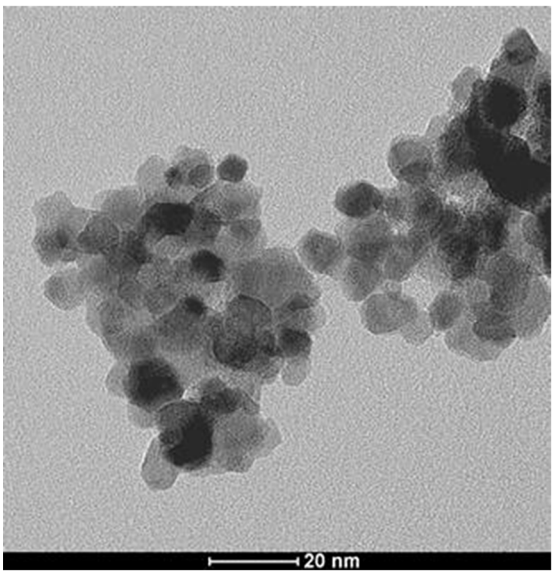

(c)

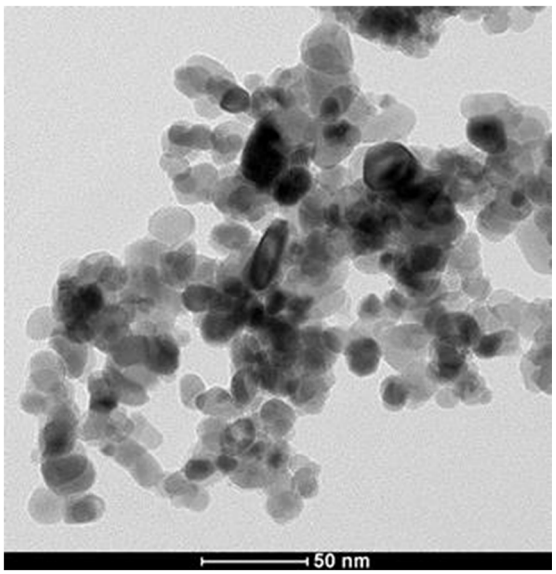

(d)

Figure 3. Characterization of commercial oxide and SnO_2 samples synthesized using different processes and calcinations temperatures, for: a) XRD patterns, b) Nitrogen adsorption-desorption isotherms,c) TEM images of O1A and d) TEM images of O3B.

Table 2. Chemical, textural and morphological characterization and band gap of SnO2 for different synthesis methods and temperatures.

SnO_2Sample	TEM	XRD	EDX		DRS	BET	BJH
	Particle Size	Crystallite Size	Chemical Composition		Band Gap	Surface Area	Pore Volume
	S_p	S_c	Sn	O	Eg	S_{BET}	V_{BJH}
	(nm)	(nm)	wt%		(eV)	(m^2g^{-1})	(cm^3g^{-1})
COM	54 ± 13	62	76	24	4.0	-	-
O1A	8 ± 1	7	70	30	3.3	-	-
O1B	18 ± 4	17	70	30	3.5	16±1	0.09
O2A	19 ± 3	19	78	22	3.8	14±1	0.03
O3A	13 ± 3	16	77	23	3.6	49±3	0.11
O3B	13 ± 3	16	77	22	3.9	50±3	0.11

However, Choudhary et al.[26] observed smaller crystallites in doped samples, likely because Pd elements are situated between the SnO_2 particles and inhibit the growth of the particles.

Figure 3 (b) illustrates the N_2 adsorption and desorption isotherms of SnO_2. All the samples exhibited type IV isotherms with type H2 hysteresis, according to IUPAC classification. The mesoporous structure of the samples determines the origin of the type IV isotherm[27]. Shalan et al.[28] reported a decline in the volume of the gas adsorbed with an increase in calcination temperature. The authors also observed that this led to a reduction in specific surface area and pore volume (O1B and O2A) due to changes in the sample particle size (Table 2).

With respect to pore size distribution, we recorded a range of 2.5-10 nm for samples O3A and O3B, while the larger particles in O1B and O2A showed a higher and wider range (12.5-27.5 nm). New pore formation may explain the two peaks observed for sample O3B (Supplementary Figure S3) due to incorporation of the dopant[29].

The aggregated particles observed in the FESEM images (Supplementary Figure S4), prompted TEM analyses. Morphological analysis using TEM indicated a nanoparticle size distribution of 8-54 nm (Supplementary Figure S5), samples O1A and O3B (Figure 3 c and d) displaying the smallest particles (8-13 nm). These findings and the XRD results corroborate those of Gaber et al.[30], whereby nanoparticle size depends on calcination temperature, exhibiting a higher degree of aggregation with an increase in particle size. According to the authors, rapid nanoparticle growth may also be the cause. A comparison of the synthesis methods for samples obtained using a calcination temperature of 400 ºC indicated smaller particles for O1A when compared to O3A and O3B, with no influence observed for the dopant. With respect to the samples calcined at 600 ºC, O1B and O2A showed similar particles sizes (18-19 nm), with values within the standard deviation.

The results of band gap determination (Table 2) indicated similar synthesized nanoparticle values (3.3-3.9 eV) to those reported by Wongsaprom et al.[23] (3.4-3.7 eV), regardless of the method used. The authors also recorded higher band gap values for samples with large particles, demonstrating that different calcination temperatures affect this property, influencing the formation of defects and increasing oxygen vacancies, leading to a rise in carrier concentration. The band gap is an important electronic parameter in characterizing solid materials because it influences semiconductor properties[31].

3.2 Zeolite characterization

Morphological analysis (FESEM) of the zeolite powder and pellet sample (Figure 4 a and b) indicated that pelletizing did not significantly affect the surface structure of the zeolite. Akhtar and Bergstrom[32] reported the same findings, even for high-temperature (800 ºC) heat treatment. Figure 4 (b) shows different structures resulting from the presence of the binder (bentonite) in the pellets.

The diffractograms in Figure 4 (c) show diffraction peaks for the pellets prepared using zeolite 13X that are consistent with the phases of commercial zeolite 13X (JCPDS #38-237), demonstrating that pelletizing did not change its structure for any of the samples. We found no new diffraction peaks, indicating no new crystalline phase formation. This is a significant result since zeolite degradation can affect their adsorption capacity[33].

The water vapor uptake test indicated differences in moisture absorption between the pellets and zeolite powder (Supplementary Figure S6). The moisture adsorption capacity in pellets (27%) was slightly lower when compared to zeolite powder (32%), demonstrating that the binding agent does not significantly absorb moisture. In both the pellets and powder samples, adsorption increased sharply up to 50 min, with saturation after 30 h. According to Fakin et al.[34], water initially adsorbs onto the outer layer of zeolites, followed by diffusion through the pores, showing signs of resistance against the transfer of moisture inside the material over time.

Gradually applying heat reverses moisture adsorption from zeolites, which leaves the crystalline structure permeated by micropores intact[35], if the heating occurs slowly and step by step. This hydrophilic characteristic of zeolites, associated with their regeneration in the form of pellets, may be important in eliminating moisture from sensor systems that might be sensitive to water vapor.

3.3 Sensor assembly

We assembled the sensor in two stages, beginning with deposition of the platinum electrodes and heaters, followed by tin dioxide. The platinum electrodes and heaters were evenly deposited onto the alumina substrate (Supplementary Figure S7) using stainless steel sputter deposition masks. We then submitted the electrode (S1B) and heater (S2A) covers to FESEM analysis (Figure 5 a and b), showing complete coverage except for the site where the masks were located. EDX analysis (Figure 5 c and d) revealed the presence of platinum at the electrode deposition site and no platinum in the region covered by the mask. These results indicate that the technique used led to adequate deposition, with the oxide adhering to the substrate.

The deposition method used produced SnO_2 films with good dispersion over the Pt electrodes, especially for oxides with small particles (8 nm, O1A) compared to those exhibiting large particles (Figure 1). The highest film thickness occurred for sensors S1B and S2A (145 and 142 µm, respectively), made using the oxides with the largest particles, when compared to S1A (73 µm), S3A (79 µm), $S3B^1$ (44 µm) and $S3B^2$ (75 µm), the last sensor showing the largest number of depositions. This study recorded higher film thicknesses than those reported by Bakrania et al.[17], who obtained film thickness of approximately 25 µm using

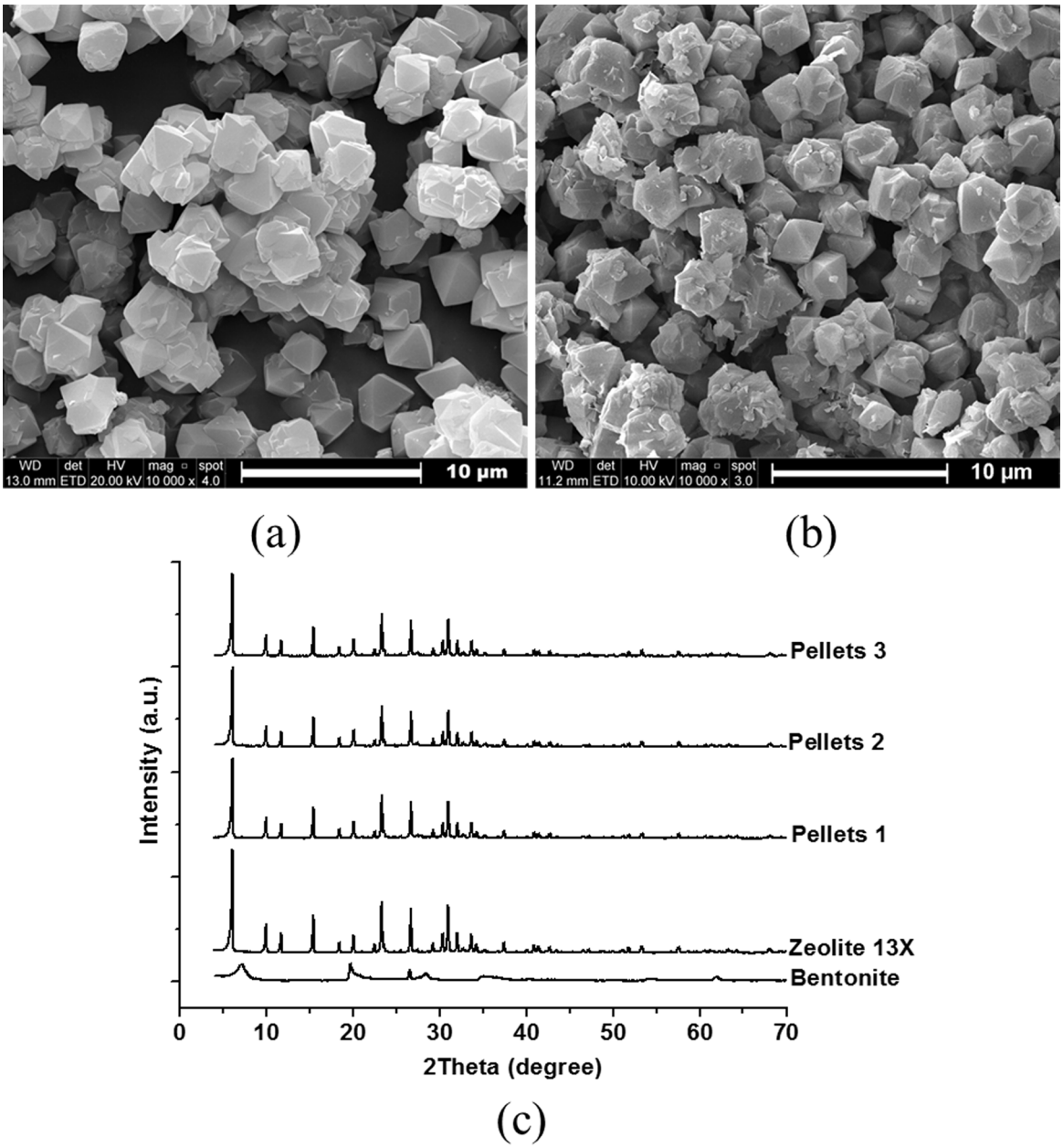

Figure 4. Characterization of 13X zeolite by: a) FESEM of zeolite 13X powder, b) FESEM of zeolite 13X pellets; and c) XRD patterns of bentonite, pellets and powder of 13X zeolite.

the same deposition method. Vilaseca et al.[36] also observed greater aggregate formation in samples with larger particles.

The thickness of the oxide layer is a parameter that can influence the sensitivity of a sensor device, where thick-film tends to be more sensitive. This is because the diffusion of the gas through the detection layer is lower in thick-films, facilitating surface reactions[37].

3.4 Sensor performance tests

We evaluated sensor sensitivity at a higher concentration range to determine the efficiency of the device within a range closer to the explosive limits of methane (5-15%). We also tested the methane detection capacity of the sensors at low concentrations, since there is a significant variation in CH_4 levels in the location intended for their application (coal mines), depending on the mine assessed. According to the Mine Safety and Health Administration[38], in the United States a mine must close if there is 1.5% (15,000 ppm) or more CH_4 in the air.

Figure 6 (a-c) shows the variation in electrical resistance (ohm) of the sensor for different methane concentrations (~4,000-36,000 ppm), with measurements taken by applying a

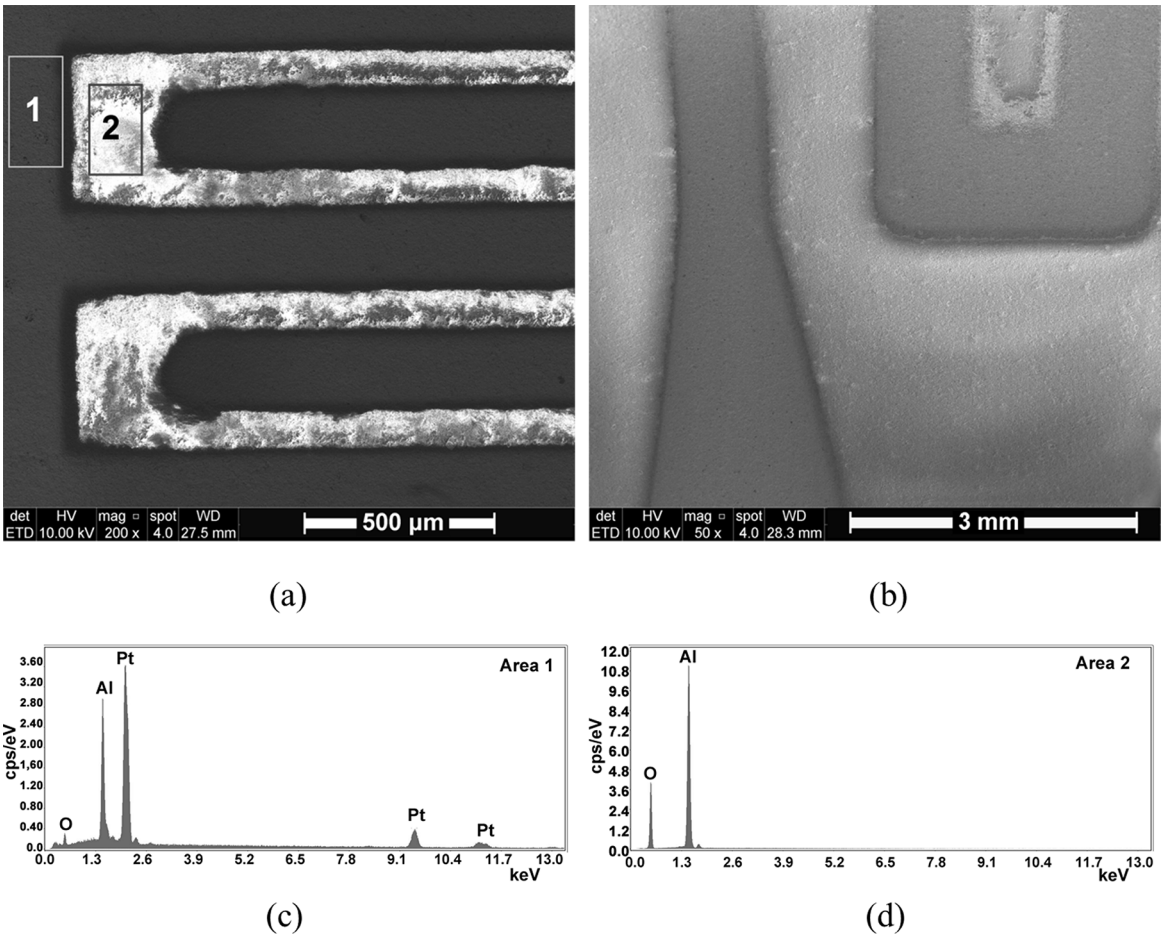

Figure 5. Sensor surface analysis for a) FESEM of the S1B electrode, b) FESEM of the S2A heater, c) EDX spectrum of the S1B electrode (point 1), d) EDX spectrum of the S1B electrode (point 2), e) FESEM of the SnO_2 film of sensor S1A.

10 V voltage at 80 ºC. Electrical resistance varied significantly for all the sensors, which detected CH_4 at all the levels tested. It is important to emphasize that the temperature used is low, compared to those usually applied[39,40], which favors their application in coal mines, since high temperatures can compromise safety due to the presence of combustible gases.

Haridas and Gupta[4] reported that sensor S1A showed a more stable baseline (R_a) during CH_4 suppression in a consecutive test with different concentrations, indicating better stability (Figure 6 a-c). Sensor S3B[1] also exhibited good stability while sensor S2A was the least stable, with the presence of significant noise at baseline. According to Miller et al.[41], this behavior is due to the variation in crystallinity, oxide particle size and band gap (Table 2).

The significant electrical resistance variations in the sensors tested demonstrated higher purity and higher band gap values in the synthesized SnO_2 samples, enabling their application in the manufacture of solid-state sensors for methane detection. As expected, the oxide (O1A) with the lowest band gap value (3.3 eV) was the most stable.

Figure 7 (a and b) shows the results of sensitivity (%) and response (Ra/Rg) for all sensors monitored at two temperatures (65 ºC and 80 ºC). We observed high sensitivities (80 - 70%) in three sensors at the highest temperature tested, with sensor S3B[1] exhibiting the best performance (Figure 7 a). The decrease in temperature to 65 ºC caused a significant decline in sensitivity (30-40%). Biaggi-Labiosa et al.[42] also reported that operating temperature significantly influenced sensor sensitivity, whereby the greatest sensitivity occurred at 300 ºC, declining at higher temperatures. According to Wang et al.[15], higher reaction rates on the surface of the oxide at elevated temperatures cause a significant increase in sensitivity.

Sensor S3B[1] performed best at 80 ºC. In addition to having a small particle size (S3B, 13 nm), it was doped with Pd, which according to Wang et al.[3], acts as oxidation catalyst and improves the reactions on the surface of the sensor. On the other hand, the increased sensitivity observed in sensor S1A is probably due to the smaller SnO_2 oxide particles (O1A, 8 nm) used in this sensor. According to

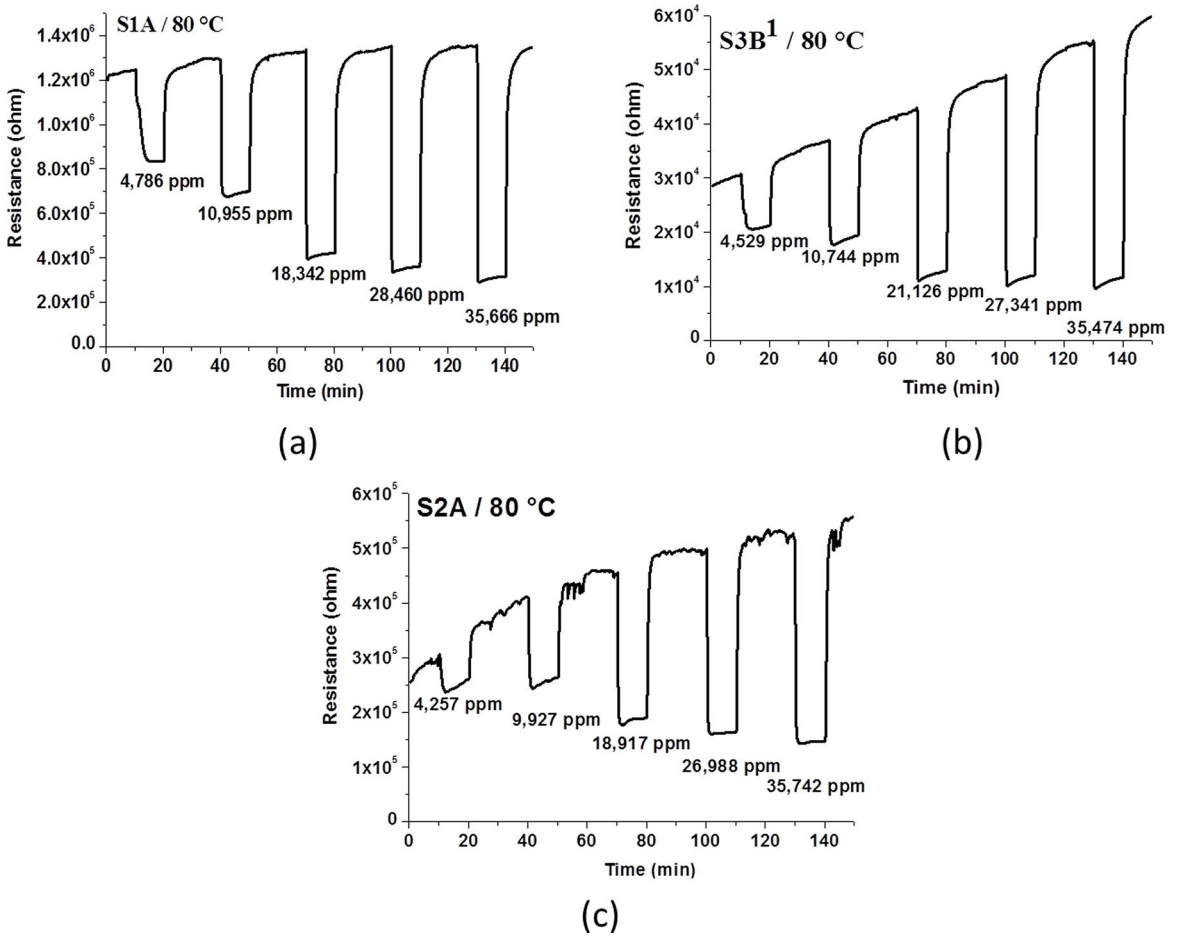

Figure 6. Electrical resistance versus time for different SnO_2 nanoparticle sensors at different CH_4concentrations in synthetic air at 10 V, for: a) S1A at 80 ºC, b) $S3B^1$ at 80 ºC and c) S2A at 80 ºC.

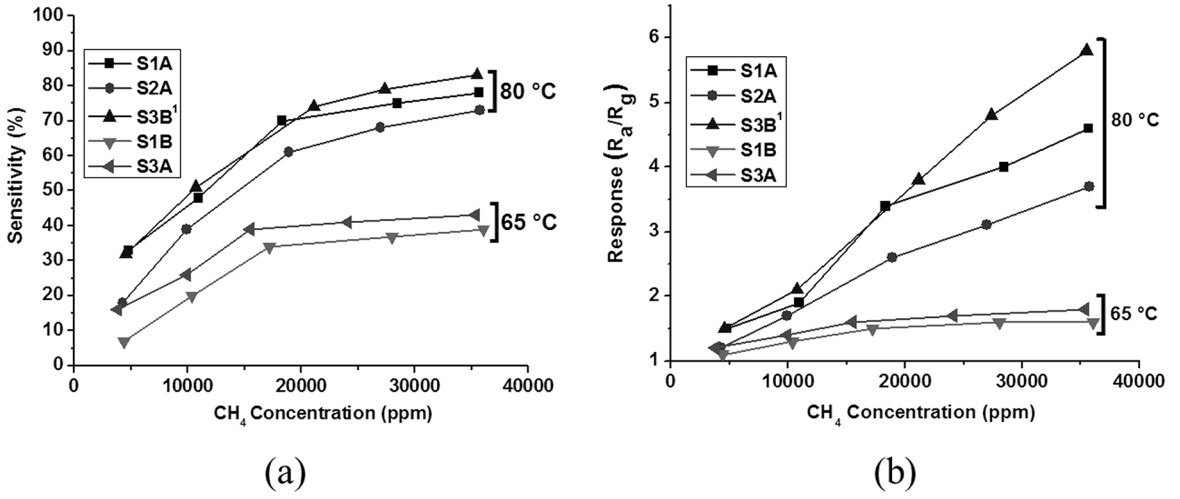

Figure 7. Gas sensor properties at different CH_4 concentrations for: a) Sensitivity at 65 and 80 ºC, and b) Response at 65 and 80 ºC.

Wang et al.[15], small particles influence the mobility of free charge carriers, with the potential to significantly improve sensitivity of metal oxide gas sensors.

Response (Ra/Rg) is an important parameter for sensor evaluation and Figure 7 (b) presents the results for the sensors tested. As expected, increasing both the gas concentration and the temperature tested produced the best results. The response values of sensors tested at 36,000 ppm were 3.5-6.0 at 80 ºC, and from 1.0 to 1.2 at at 65 ºC. Min and Choi[43] recorded a more significant response (Ra/Rg = 2.3) to CH_4

(5,000 ppm) in an SnO_2 sensor at an operating temperature of 400 ºC using a platinum film (4.5 nm thick), when compared to the same sensor without the Pt film (Ra/Rg 1.8). The last response is similar to that observed for sensors S1A and S3B[1] (Ra/Rg 1.5) at 80 ºC for the same CH_4 concentration (5,000 ppm) (Figure 7 b). This result confirms the good performance of the sensors produced in the present study.

Figure 8 (a) shows the variations in electrical resistance (ohm) over a wide temperature range (20 up to 90 ºC) for sensor S3B[2], tested at a CH_4 concentration of 4,700 ppm. Once again, there was a significant change in electrical resistance according to the operating temperature. Sensitivity increased significantly from 0.03% at 20 ºC to 86% at 90 ºC. A second test at 90 ºC, with sensitivity of 87%, reproduced this result. We assessed the electrical resistance of this sensor, with a thicker SnO_2 film (Figure 8 b) at different gas concentrations (179 - 2,559 ppm) and constant temperature (90 ºC). The S3B[2] sensor exhibited a greater measurable change in electrical resistance, without significant signal noise at 179 ppm of CH_4. It continued to show a significant response at the other concentrations assessed, with sensitivity varying from 15 to 82%.

Assessment of the influence of film thickness on the sensor signal improves by comparing the results obtained for two sensors made with the same SnO_2 oxide (O3B, Table 1). The thicker SnO_2 film increased the sensitivity of S3B[2] (75 µm, 73% at 4,827 ppm) when compared to S3B[1] (44 µm, 32% at 4,529 ppm) analyzed at 80 ºC (previous test). Vuong et al.[39] also observed higher sensitivity for CH_4 in sensors with thicker SnO_2 films (200 nm ~40%, 300 nm ~65%), using nickel oxide as a catalyst. The thickness of the oxide film can influence sensor sensitivity, with thicker films tending to be more sensitive.

Two of the basic criteria for gas sensors are response time and recovery time. For most practical applications, one must not only estimate the target gas concentration, but also identify it quickly. The long recovery period needed after gas exposure restricts their use in applications where gas concentrations may change rapidly[2]. We assessed response and recovery times (Supplementary Figure S8) to methane concentration in S3B[2] at 90 ºC and low CH_4 levels (179-2,559 ppm), with response time decreasing as the concentration increased, in line with Biaggi-Labiosa et al.[42], with the opposite occurring for recovery time. Response times were between 25 and 257 s, consistent with the findings of these authors, who reported response times of 120-168 s for an SnO_2 sensor at concentrations of 125-2,500 ppm and temperature of 100 ºC. The results indicate that the sensor responds quickly when exposed to higher gas concentrations. Reactions that occur on the surface of the oxide determine response and reaction times; for example, the use of catalysts reduces the activation energy needed for a surface reaction, decreasing response and recovery times[41].

Good CO_2 selectivity is an important advantage of the proposed sensor, since carbon dioxide is present in coal mine air[21] and is the major interferent in determining the CH_4 concentration in these environments. According to Wang et al.[15], CO_2 behaves like a weak reducing gas when in contact with an n-type sensor (SnO_2), with detection increasing at concentrations between 5,000 and 10,000 ppm and high temperatures (240 ºC).

Figure 9 (a) shows the variation in electrical resistance of S1A for CO_2 (2,050 ppm) and CH_4 (20,109 ppm), with a decline in electrical resistance for both gases, mirroring the behavior of n-type sensors in the presence of a reducing gas. This result demonstrates that S1A exhibits sensitivity to CO_2 (8.7%), which could interfere in CH_4 analysis. Xiong et al.[44] also reported sensitivity to CO_2 (9%) in a non-doped SnO_2 sensor.

We tested the same sensor again under the same conditions, but using a zeolite 13X filter in front of the device (Figure 9 b). Electrical resistance did not display the aforementioned behavior with CO_2 alone (2,551 ppm). Electrical resistance declined upon contact with CH_4 when

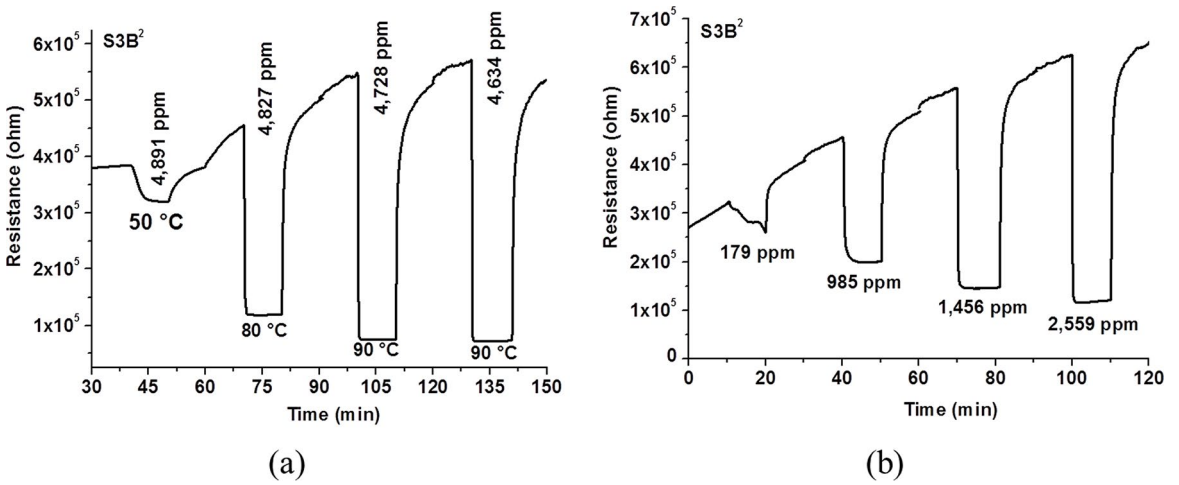

Figure 8. Gas sensor properties for a) Electrical resistance versus time at different operating temperatures, and b) Electrical resistance versus time at low CH_4 concentrations.

testing involved a gas mixture (CO_2 + CH_4), indicating that zeolite 13X pellets did not interfere in the methane signal. We obtained similar methane values when monitoring CH_4 concentration by gas chromatography before and after contact with the pellets, demonstrating that no adsorption took place. By contrast, zeolite almost completely adsorbed CO_2 (from 1,699 to 17 ppm), indicating that CO_2 does not interfere in the methane signal of the sensor. As such, the sensor is more selective and capable of detecting CH_4 even in the presence of CO_2 (1,669 ppm).

The high zeolite adsorption capacity of CO_2 in relation to CH_4 is due to differences in electrical properties[45]. CO_2 has a large quadrupole moment, resulting in strong interaction with the adsorbent surfaces of zeolite 13X[46]. By contrast, CH_4, which is a non-polar molecule, may adsorb to the adsorbent surface only at a sufficiently high pressure[45].

Table 3 shows a summary of the sensitivity values, and response and recovery times of sensors for ~20,000 ppm of CH_4 (2.5 times lower than the explosive range) at different operating temperatures (65 and 80ºC). Biaggi-Labiosa et al.[42] recorded a longer response time for sensors tested at low temperatures. The response times at 80 ºC were lower than those Nikmanesh et al.[40] observed (65 s for non-doped SnO_2 sensors and 34 s for those doped with tungsten carbide). Nasresfahani et al.[47] reported response times of 300-420 s for Pd doped CH_4 sensors, operated at room temperature, much higher than those we recorded at 65 ºC.

In the present study, all the sensors tested at 80 ºC showed a response time shorter than 30 s at this CH_4 concentration. Sensor structures based on oxide semiconductors reported in the literature showed response times longer than 10 s and recovery of more than 40 s for CH_4 detection[40]. These authors found that nanostructured doped sensors can affect sensitivity as well as response and recovery times. In this study, sensors with smaller particles (S1A) doped with palladium (S3B[1]) exhibited shorter response and recovery times when exposed to ~20,000 ppm of CH_4.

4. Conclusions

Synthesis by Sn(s) oxidation and chemical precipitation at a low calcination temperature (O1A and O3B) was the most promising synthesis method in producing a solid-state sensor, since it exhibits the smallest particle size and a band gap value similar to that reported in the literature.

With respect to solid-state sensors, electrical resistance declined in all the tests conducted, demonstrating n-type behavior in SnO_2 in contact with methane. Initial tests at room temperature (20 ºC) showed sensitivity to CH_4 even at low temperatures. When we exposed the sensors to higher temperatures (65 ºC), sensor properties rose significantly, improving at 80 and 90 ºC, exhibiting high sensitivity, detection of low methane concentrations, short response and recovery times, and signal reproducibility.

The best performance occurred in sensors S1A, S3B[1] and S3B[2]. Sensor S1A exhibited greater baseline stability, as did S3A, despite the latter being assessed at a lower temperature (65 ºC). The excellent properties in detecting CH_4 are due

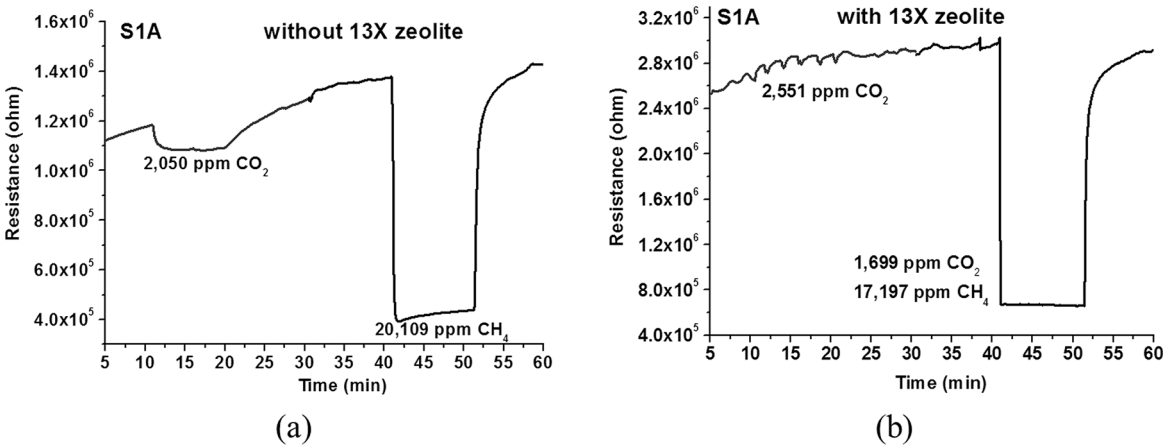

Figure 9. Electrical resistance versus time for CO_2 and CH_4 analyzed by sensor S1A without (a) and with (b) 13X zeolite pellets filter.

Table 3. Performance of the different sensors exposed to ~20,000 ppm CH_4.

Sensor	SnO_2Sample	CH_4 Conc.	Sensitivity	Response Time	Recovery Time	Temperature
		(ppm)	(%)	(s)	(s)	(°C)
S1B	O1B	17,236	34	111	95	65
S3A	O3A	15,486	39	76	88	65
S1A	O1A	18,342	70	14	55	80
S3B[1]	O3B	21,126	74	16	70	80
S2A	O2A	18,917	61	29	47	80

to the presence of Pd in S3B[1] and S3B[2] and small particle sizes in both devices. Pd doping can significantly improve sensitivity to CH_4 at low operating temperatures because of its high catalytic activity, while the smaller particle size of SnO_2 can increase sensitivity because the surface area in contact with the gas influences transducer performance.

The improved selectivity of sensor S1A resulted from using zeolite 13X pellets as a filter to remove CO_2. The zeolite 13X pellets allowed the sensor to selectively detect methane even in the presence of CO_2 levels similar to those found in coal mines. Zeolite 13X proved to be efficient at adsorbing moisture, demonstrating its potential for applications in sensors used in locations where moisture is present.

Given that reducing the operating temperature of these devices is an urgent task in detecting methane without compromising occupational safety, the results obtained are promising for the application of this device to detect CH_4 in coal mines.

5. Acknowledgments

The authors are grateful to the CNPq (National Council for Scientific and Technological Development, grant number 312323/2015-8 and 490218/2012-1 to M. J. R. Pires) for funding the project. R. C. Abruzzi thanks PUCRS (Pontifical Catholic University of Rio Grande do Sul), FAPERGS (Research Support Foundation of Rio Grande do Sul) and CAPES (Coordination for the Improvement of Higher Education Personnel, for Ph.D grant number 3842.283.15928.22032013-015/2012). The authors would also like to thank Dr. C. Bayer (Federal University of Rio Grande do Sul) for donating the commercial sampling flasks.

6. References

1. Das S, Jayaraman V. SnO2: A comprehensive review on structures and gas sensors. *Progress in Materials Science*. 2014;66:112-255.
2. Neri G. First Fifty Years of Chemoresistive Gas Sensors. *Chemosensors*. 2015;3(1):1-20.
3. Wang C, Yin L, Zhang L, Xiang D, Gao R. Metal Oxide Gas Sensors: Sensitivity and Influencing Factors. *Sensors (Basel)*. 2010;10(3):2088-2106.
4. Haridas D, Gupta V. Study of collective efforts of catalytic activity and photoactivation to enhance room temperature response of SnO_2 thin film sensor for methane. *Sensors and Actuators B: Chemical*. 2013;182:741-746.
5. Bochenkov VE, Sergeev GB. Sensitivity, Selectivity, and Stability of Gas-Sensitive Metal-Oxide Nanostructures. In: Umar A, Hahn YB, eds. *Metal Oxide Nanostructures and Their Applications*. Volume 3. Valencia, CA: American Scientific Publishers; 2010. p. 31-52.
6. Graunke T, Schmitt K, Wöllenstein J. Organic Membranes for Selectivity Enhancement of Metal Oxide Gas Sensors. *Journal of Sensors*. 2016;2016:2435945.
7. Thommes M, Mitchell S, Pérez-Ramirez J. Surface and Pore Structure Assessment of Hierarchical MFI Zeolites by Advanced Water and Argon Sorption Studies. *The Journal of Physical Chemistry C*. 2012;116(35):18816-18823.
8. Hugon O, Sauvan M, Benech P, Pijolat C, Lefebvre F. Gas separation with a zeolite filter, application to the selectivity enhancement of chemical sensors. *Sensors and Actuators B: Chemical*. 2000;67(3):235-243.
9. Thakur P. Coal Seam Degasification. In: Thakur P, Schatzel S, Aminian K, eds. *Coal Bed Methane - From Prospect to Pipeline*. San Diego: Elsevier; 2014. p. 155-175.
10. Speight JG. *Handbook of Coal Analysis*. Hoboken: John Wiley & Sons; 2015.
11. Sergent N, Gélin P, Périer-Camby L, Praliaud H, Thomas G. Preparation and characterisation of high surface area stannic oxides: structural, textural and semiconducting properties. *Sensors and Actuators B: Chemical*. 2002;84(2-3):176-188.
12. Senthilkumar V, Vickraman P, Ravikumar R. Synthesis of fluorine doped tin oxide nanoparticles by sol-gel technique and their characterization. *Journal of Sol-Gel Science and Technology*. 2010;53(2):316-321.
13. Nandan B, Venugopal B, Amirthapandian S, Panigrahi BK, Thangadurai P. Effect of Pd ion doping in the band gap of SnO_2 nanoparticles: structural and optical studies. *Journal of Nanoparticle Research*. 2013;15:1999.
14. Abruzzi RC, Bonetti B, Pires MJR, Dedavid BA, Cardoso AM, Luvizon NS. *The Influence of Pelletization in Water Vapor and CO_2 Adsorption at Different Zeolites*. In: 18th International Zeolite Conference - IZC; 2016 Aug 19-24; Rio de Janeiro, RJ, Brazil. p. 1-2.
15. Wang D, Chen Y, Liu Z, Li L, Shi C, Qin H, et al. CO_2-sensing properties and mechanism of nano-SnO_2 thick-film sensor. *Sensors and Actuators B: Chemical*. 2016;227:73-84.
16. Rongsayamanont C, Sopajaree K. *Modification of Synthetic Zeolite Pellets from Lignite Fly Ash A: The Pelletization*. In: World of Coal Ash - WOCA; 2007 May 7-10; Northern Kentucky, USA.
17. Bakrania SD, Wooldridge MS. The Effects of Two Thick Film Deposition Methods on Tin Dioxide Gas Sensor Performance. *Sensors (Basel)*. 2009;9(9):6853-6868.
18. Oros C, Horprathum M, Wisitsoraat A, Srichaiyaperk T, Samransuksamer B, Limwichean S, et al. Ultra-sensitive NO_2 sensor based on vertically aligned SnO_2 nanorods deposited by DC reative magnetron sputtering with glancing angle deposition technique. *Sensors and Actuators B: Chemical*. 2016;223:936-945.
19. Karacan CO, Ruiz FA, Cotè M, Phipps S. Coal mine methane: A review of capture and utilization practices with benefits to mining safety and to greenhouse gas reduction. *International Journal of Coal Geology*. 2011;86(2-3):121-156.
20. Abruzzi RC, Bonetti B, Pires MJR, Dedavid BA, Bitencourt AK. Artifacts in the Analysis and Assessment of Low-Cost Containers for Sampling and Storing Greenhouse Gases. *Química Nova*. 2019;42(1):84-94.

21. Bonetti B, Abruzzi RC, Pires MJR, Dedavid BA, Bitencourt AK, Gomes CJB. *Monitoring CH_4, CO_2 and CO Concentrations on the Air of the Underground Coal Mines in Southern Brazil*. In: 24th World Mining Congress - WMC; 2016 Oct 18-21; Rio de Janeiro, RJ, Brazil.

22. Li C, Lv M, Zuo J, Huang X. SnO2 highly sensitive CO gas sensor based on quasi-molecular-imprinting mechanism design. *Sensors (Basel)*. 2015;15(2):3789-3800.

23. Wongsaprom K, Bornphotsawatkun R, Swatsitang E. Synthesis and characterization of tin oxide (SnO_2) nanocrystalline powders by a simple modified sol-gel route. *Applied Physics A*. 2014;114(2):373-379.

24. Son HH, Lee WG. Effect of rapid thermal annealing process on calcination of tin oxide powder. *Surface and Interface Analysis*. 2012;44(8):989-992.

25. Aziz M, Abbas SS, Baharom WRW. Size-controlled synthesis of SnO_2 nanoparticles by sol-gel method. *Materials Letters*. 2013;91:31-34.

26. Choudhary M, Mishra VN, Dwivedi R. Solid-state reaction synthesized Pd-doped tin oxide thick film sensor for detection of H_2, CO, LPG and CH_4. *Journal of Materials Science: Materials in Electronics*. 2013;24(8):2824-2832.

27. Gregg SJ, Sing KSW. *Adsorption, Surface Area, and Porosity*. London: Academic Press; 1982.

28. Shalan AE, Osama I, Rashad MM, Ibrahim IA. An investigation on the properties of SnO_2 nanoparticles synthesized using two different methods. *Journal of Materials Science: Materials in Electronics*. 2014;25(1):303-310.

29. Yang H, Song X, Zhang X, Ao W, Qiu G. Syntehsis of vanadium-doped SnO_2 nanoparticles by chemical co-precipitation method. *Materials Letters*. 2003;57(20):3124-3127.

30. Gaber A, Abdel-Rahin MA, Abdel-Latief AY, Abdel-Salam MN. Influence of Calcination Temperature on the Structure and Porosity of Nanocrystalline SnO_2 Synthesized by a Conventional Precipitation method. *International Journal of Electrochemical Science*. 2014;9:81-95.

31. López R, Gómez R. Band-gap energy estimation from diffuse reflectance measurements on sol-gel and commercial TiO_2: a comparative study. *Journal of Sol-Gel Science and Technology*. 2012;61(1):1-7.

32. Akhtar F, Bergström L. Colloidal Processing and Thermal Treatment of Binderless Hierarchically Porous Zeolite 13X Monoliths for CO_2 Capture. *Journal of the American Ceramic Society*. 2011;94(1):92-98.

33. Sebastian J, Peter SA, Jasra RV. Adsorption of Nitrogen, Oxygen, and Argon in Cobalt(II)-Exchanged Zeolite X. *Langmuir*. 2005;21(24):11220-11225.

34. Fakin T, Ristic A, Horvat A, Kaucic V. *Water Adsorption Study on the Zeolite LTA Granules*. In: 5th Serbian-Croatian-Slovenian Symposium on Zeolites; 2013 May 30-Jun 2; Zlatibor, Serbia.

35. Flanigen EM. Zeolites and molecular sieves. An historical perspective. In: Van Bekkum H, Flanigen EM, Jacobs PA, Jansen JC, eds. *Studies in Surfaces Science and Catalysis. Introduction to Zeolite Science and Practice*. Amsterdam: Elsevier; 2001. p. 11-36.

36. Vilaseca M, Coronas J, Cirera A, Cornet A, Morante JR, Santamaria J. Gas detection with SnO_2 sensors modified by zeolite films. *Sensors and Actuators B: Chemical*. 2007;124(1):99-110.

37. Becker T, Ahlers S, Braunmühl CB, Müller G, Kiesewetter O. Gas sensing properties of thin- and thick-film tin-oxide materials. *Sensors and Actuators B: Chemical*. 2001;77(1-2):55-61.

38. Mine Safety and Health Administration - MSHA. *Rules and Regulations U.S., Federal Register*. Volume 66, n. 13. Arlington: MSHA; 2001. p. 1-182.

39. Vuong NM, Hieu NM, Hieu HN, Yi H, Kim D, Han YS, et al. Ni_2O_3-decorated SnO_2 particulate films for methane gas sensors. *Sensors and Actuators B: Chemical*. 2014;192:327-333.

40. Nikmanesh S, Doroodmand MM, Sheikhi MH, Zarifkar A, Zahabi A. *Specific CH_4 gas sensor based on tungsten carbide/SnO_2 core-shell modified interdigitated electrode*. In: 21st Iranian Conference on Electrical Engineering - ICEE; 2013 May 14-16; Mashhad, Iran.

41. Miller DR, Akbar SA, Morris PA. Nanoscale metal oxide-based heterojunctions for gas sensing: A review. *Sensors and Actuators B: Chemical*. 2014;204:250-272.

42. Biaggi-Labiosa A, Solá F, Lebrón-Colón M, Evans LJ, Xu JC, Hunter GW, et al. A novel methane sensor based on porous SnO_2 nanorods: room temperature to high temperature detection. *Nanotechnology*. 2012;23(45):455501.

43. Min BK, Choi SD. Undoped and 0.1 wt% Ca-doped Pt-catalyzed SnO_2 sensors for CH_4 detection. *Sensors and Actuators B: Chemical*. 2005;108(1-2):119-124.

44. Xiong Y, Xue Q, Ling C, Lu W, Ding D, Zhu L, et al. Effective CO_2 detection based on LaOCl-doped SnO_2 nanofibers: Insight into the role of oxygen in carrier gas. *Sensors and Actuators B: Chemical*. 2017;241:725-734.

45. Pour AA, Sharifnia S, Salehi RN, Ghodrati M. Adsorption separation of CO_2/CH_4 on the synthesized NaA zeolite shaped with montmorillonite clay in natural gas purification process. *Journal of Natural Gas Science and Engineering*. 2016;36(Pt A):630-643.

46. Mulgundmath VP, Tezel FH, Saatcioglu T, Golden TC. Adsorption and separation of CO_2/N_2 and CO_2/CH_4 by 13X zeolite. *The Canadian Journal of Chemical Engineering*. 2012;90(3):730-738.

47. Nasresfahani S, Sheikhi MH, Tohidi M, Zarifkar A. Methane gas sensing properties of Pd-doped SnO_2/reduced graphene oxide synthesized by a facile hydrothermal route. *Materials Research Bulletin*. 2017;89:161-169.

Supplementary material

The following online material is available for this article:

Figure S1. Drawing for the manufacture of a sputter deposition mask, in: a) electrode; and b) heater.

Figure S2. FTIR spectra of commercial oxide and SnO_2 samples synthesized using different processes and calcination temperatures.

Figure S3. Pore size distribution of SnO_2 samples synthesized using different processes and calcination temperatures.

Figure S4. FESEM micrographs of SnO_2 nanoparticles synthesized using different methods and calcination temperatures and the commercial sample, in: a) O1A, b) O1B, c) O2A, d) O3A, e) O3B and f) COM.

Figure S5. TEM images of commercial samples and SnO_2 nanoparticles synthesized using different methods and calcination temperatures, for: a) O1B, b) O2A, c) O3A and d) COM.

Figure S6. Moisture adsorption in zeolite pellets. *CP_13X: Commercial zeolite 13X pellets.

Figure S7. Alumina substrates deposited with platinum heaters, platinum electrodes, and deposition of SnO_2 films on the electrodes.

Figure S8. Response and recovery times for the $S3B^2$ sensor at low concentrations at 90°C.